OTC 20002

Scenario-Based Assessment of Risks to Ice Class Ships

A. Kendrick and B. Quinton, BMT Fleet Technology Limited, and C.G. Daley, Memorial University of Newfoundland

This paper was prepared for presentation at the 2009 Offshore Technology Conference held in Houston, Texas, USA, 4–7 May 2009.

Abstract

The rise in resource related projects in the Arctic has created the need for new approaches to assessing and minimizing risk. The new tankers and drill ships required for the Arctic will be larger and stronger than any previous ships, but will be very carefully designed and operated. The paper presents a methodology for assessing risk to large Arctic ships in a variety of scenarios. For the purpose of illustration of the approach, two ice collision scenarios are described. One is the case of a large ship with a bulbous bow hitting an iceberg head-on. The second is an aft waterline collision with a sea ice floe. Both scenarios are outside the conditions formally considered in standard ice class rules but are significant issues. The paper provides owners/designers/regulators with an example of a methodology to examine ice loads using a rational set of design scenarios. The results show that vessels can easily be operated in a manner that can create dangerous load levels. The results are directly relevant to the structural design of new large Arctic tankers (oil and LNG) and large Arctic drill ships. The second part of the paper presents some initial results from consideration of plastic structural response to moving ice loads. The significance of the movement (sliding) of the load increases as the response level increases. Elastic responses are only slightly influenced by the movement of the load along the hull, while the larger plastic responses are greatly affected by movement. This paper is mainly intended to raise this as an issue of potential concern.

Nomenclature

An	ice crushing area
Co	mass reduction factor (Popov)
Fn	ice crushing force
IE	indentation energy
KE_e	effective kinetic energy
M_e	effective collision mass
M	collision mass
Pav	ice pressure
Po	ice strength parameter
R	paraboloid nose radius(for bulbous bow impact)
r	contact area radius (for bulbous bow impact)
ex	ice pressure-area exponent
f_A	geometry function
h	basic ice thickness
w	width of contact (aft body case)
ζ	normal ice indentation
ϕ	wedge opening angle

Introduction

Regardless of recent oil price fluctuations, the long term trend in demand for resources means that the Arctic will remain the focus of development plans in many organizations. Estimates suggest that around 25% of undiscovered global hydrocarbons are located in Arctic areas such as Russia, Canada, and Alaska. Marine transportation is an attractive option, due to the challenges in establishing fixed infrastructure in remote regions. Figure 1 illustrates some possible future Arctic transportation routes.

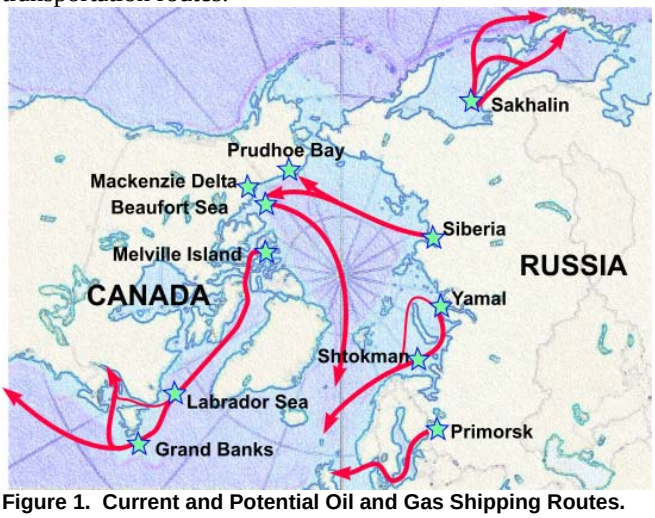

Figure 1. Current and Potential Oil and Gas Shipping Routes.

Many ice-capable ships already exist, and there is some experience of their operation in Arctic conditions. Drill ships have been deployed in the Arctic on a seasonal basis, and now there are concepts for extended season and possibly year round operations. To date no Arctic-capable LNG tankers have been built, and there are no drill ships or FPSO's capable of year-round operations. In the decades since 1985, knowledge of ice loads has increased and rules for vessels construction have become more formalized (IACS 2007). However, in cases where there are no similar ice class ships available for reference, designers, owners and regulators may need to consider 'first principles' (fundamental) approaches rather than experience-based rules. This paper presents a physics-based methodology for assessing specific ice loads on Arctic vessels. The approach treats a wide variety of scenarios, some of which have been previously reported (see Daley and Kendrick (2008), Daley, Kendrick, Yu, and Noh (2007)). Two additional ice collision scenarios are described here. One is the case of a large ship with a bulbous bow hitting an iceberg head-on (see Figure 2). The second (Figure 3) is an aft waterline collision with a sea ice floe. Both scenarios are outside the conditions formally considered in standard ice class rules but are significant issues. The paper provides owners/designers/regulators with an example of a methodology to examine ice loads using a rational set of design scenarios.

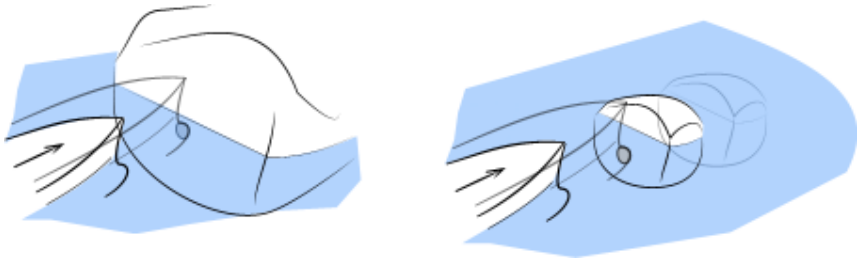

Figure 2. Iceberg and bergy bit impact on a bulbous bow.

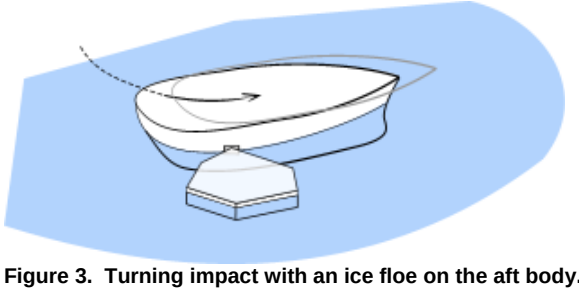

Figure 3. Turning impact with an ice floe on the aft body.

Following the presentation of the loads, a discussion of a new development in the plastic structural response of stiffened panels is presented. Ice worthy design is often based on plastic capacity, with the assumption that even beyond the notional plastic limit state there is significant plastic strength reserve. Normally the extent of this reserve is assessed by the use of non-linear finite element analysis, where typically the movement of the load during the interaction is not considered. The results presented below will show that there may be a significant loss of reserve capacity due to the movement of the load along the structure.

Impact Mechanics

The two scenarios shown above each involve ice interaction. Each case depends on the geometry of the indentation (ship and ice) and the ice crushing strength. For these scenarios, the problem is one of impact between two objects. It is assumed that one body is initially moving (the impacting body) and the other is at rest (the impacted body). The solution is found by equating the available (effective) kinetic energy with the energy expended in ice crushing. To do this, the first step is to create an equivalent system (see Figure 4). This concept was first used to calculate ice impacts by Popov et. al. (1967). The concept is valid for short duration impacts, as it ignores any sliding effects (e.g. friction), changes in potential energy or velocity related forces (e.g. drag). With these assumptions a general collision can be solved as if it were is simple normal collision (see Figure 5). The solution is found by equating the normal kinetic energy to the work done by the normal force during the impact. The peak force is assumed to occur at the maximum indentation.

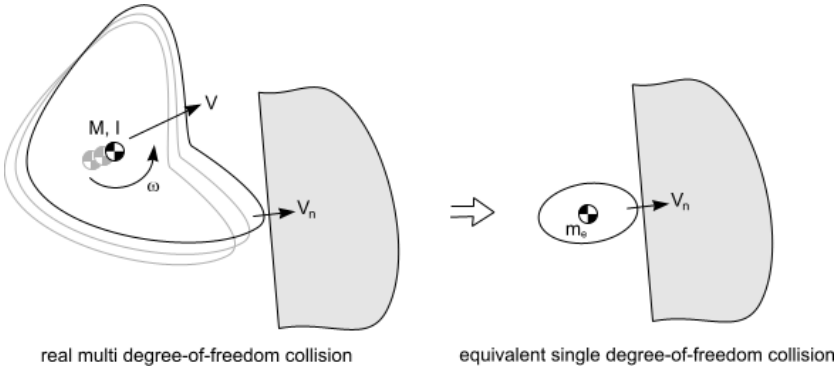

Figure 4. Concept of an equivalent system for impact analysis.

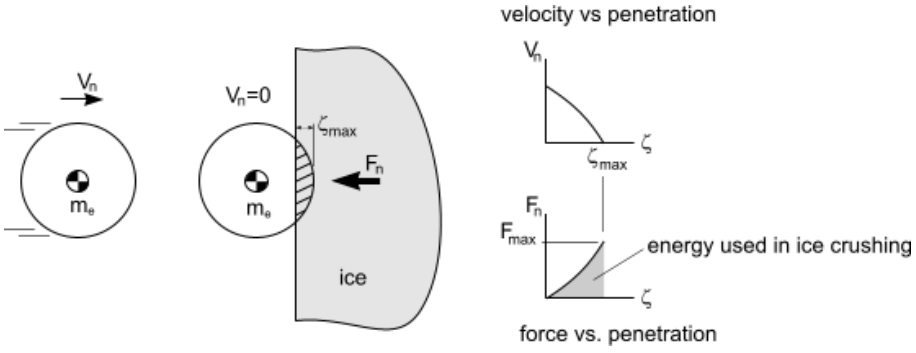

Figure 5. Impact analysis based on equating kinetic energy to work done during indentation.

This approach is fully described in Daley (1999). The energy equations require an equation that relates force to indentation. By using a pressure-area relationship to describe ice pressures, it is easy to derive a force-indentation relationship. The average pressure P_{av} and the ice force F_n are related to the normal contact area A_n as;

$$P_{av} = P_0 \cdot A_n^{ex} \quad (1)$$

$$F_n = P_{av} \cdot A_n = P_0 \cdot A_n^{1+ex} \quad (2)$$

where P_o is the pressure at $1m^2$, and *ex* is a constant. Equation (1) is a 'process' pressure area model.

For each contact situation, there is a relationship between the normal indentation ζ_n and normal contact area;

$$A_n = f_A(\zeta) \qquad (3)$$

where f_A is a function that depends on the contact geometry. This results in a function relating force to indentation;

$$F_n = Po \cdot (f_A(\zeta))^{1+ex} \qquad (4)$$

The next step is to determine the indentation energy IE, which is found by integrating the force;

$$IE = \int F_n d\zeta \qquad (5)$$

For the case of spherical contact Figure 6 shows a geometry, which will be used to describe the bulbous bow contact. The actual solution is for a paraboloid, and is only valid for shallow indentations on spheres.

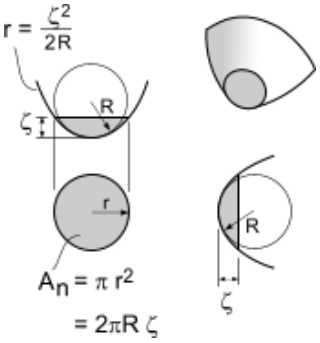

Figure 6. Contact geometry for either a sphere of radius R or a paraboloid with the same radius

The indentation energy for the spherical contact is derived as follows. The projected normal area is;

$$A_n = 2\pi \cdot R \cdot \varsigma \qquad (6)$$

The ice penetration force is:

$$F_n = p_o(2\pi \cdot R)^{1+ex} \cdot \zeta^{1+ex} \qquad (7)$$

The indentation energy is found by substituting (7) into (5), to give:

$$IE = \frac{p_o}{2+ex}(2\pi \cdot R)^{1+ex}\zeta^{2+ex} \qquad (8)$$

For the case of wedge contact Figure 7 shows a geometry, which will be used to describe the aft body contact.

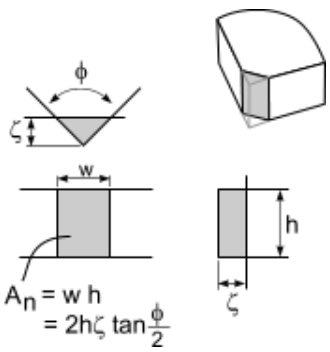

Figure 7. Contact geometry for a wedge of a level ice sheet of opening angle ϕ.

The indentation energy for the wedge contact is derived as follows. The projected normal area is;

$$A_n = 2h\tan\frac{\phi}{2}\cdot\varsigma \qquad (9)$$

The ice penetration force is:

$$F_n = p_o\left(2h\tan\frac{\phi}{2}\right)^{1+ex}\cdot\zeta^{1+ex} \qquad (10)$$

The indentation energy is found by substituting (10) into (5), to give:

$$IE = \frac{p_o}{2+ex}\left(2h\tan\frac{\phi}{2}\right)^{1+ex}\zeta^{2+ex} \qquad (11)$$

Equations (6) and (9) are both linear functions of ζ and equations (8) and (11) are very similar, only differing by a constant. The solution for z is found by equating the indentation energy (equation (8) or (11)) with the effective kinetic energy; as follows;

$$KE_e = IE \qquad (12)$$

$$KE_e = \frac{1}{2}M_e\cdot V_n{}^2 = \frac{1}{2}\frac{M}{Co}\cdot V_n^2 \qquad (13)$$

Where *Co* is the Popov mass reduction term and V_n is the normal contact velocity. After substitution of equations (13) and (11) (or (8)) into equation (12) the only unknown is ζ. The force is then found by substitution of ζ back into (10) or (7).

Bulbous Bow Loads

In the case of an open water hull form with a bulbous bow, the collision with ice will be direct and will not involve any slide-up or beaching. The collision scenario is sketched in Figure 2. The bulbous bow is assumed to strike a vertical flat face of ice.

In order to permit a direct analytical solution the approach taken is to fit a paraboloid form (a surface of revolution of a parabola), to the bulb. Figure 8 shows the parboloid superimposed on a bulbous bow.

In the case of a head on collision the normal velocity is the full vessel speed. The effective mass is found by combining the ship mass and the iceberg mass as follows (assuming a direct hit with the collision force acting through the centers of mass of both bodies);

$$M_e = \frac{1}{\frac{1}{M_{ship}}+\frac{1}{M_{ice}}} \qquad (14)$$

The energy balance is expressed in the equation;

$$\frac{1}{2}M_e\cdot V_{ship}^2 = \frac{p_o}{2+ex}(2\pi\cdot R)^{1+ex}\zeta^{2+ex} \qquad (15)$$

Solving the equation gives the penetration;

$$\varsigma = \left(\frac{2+ex}{2\cdot p_o\cdot(2\pi\cdot R)^{1+ex}}\frac{1}{\frac{1}{M_{ship}}+\frac{1}{M_{ice}}}\cdot V_{ship}^2\right)^{\frac{1}{2+ex}} \qquad (16)$$

The force is found by substituting (16) into(7);

$$F_n = p_o(2\pi \cdot R)^{1+ex} \cdot \left(\frac{2+ex}{2 \cdot p_o \cdot (2\pi \cdot R)^{1+ex}} \frac{1}{\frac{1}{M_{ship}} + \frac{1}{M_{ice}}} \cdot V_{ship}^2 \right)^{\frac{1+ex}{2+ex}} \quad (17)$$

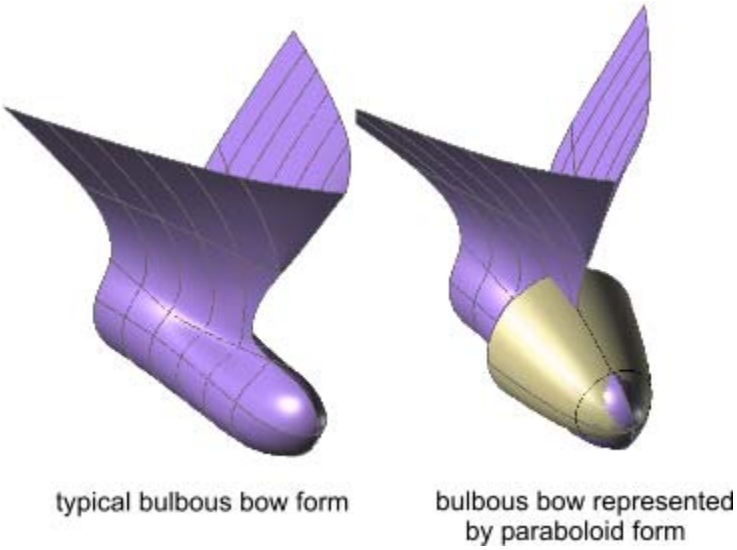

Figure 8: Simplification of Bulbous Bow with Paraboloid Form

While this equation is somewhat lengthy, it is only an algebraic function of some simple ship and ice parameters and is easily calculated. To explore this equation, a set of collisions with a vessel of 100,000 tonnes displacement is tabulated in Table 1. Figure 9 plots the influence of ship speed on the collision force. The influence is nearly linear for this case. Figure 10 shows the influence of the ice strength parameter Po, which is also close to linear. These results are only presented to indicate the types of results that are possible. A much larger sensitivity study can be undertaken for actual design cases. The values of the parameters presented here are only for illustration of the mechanics, and are not suggested as appropriate design values. Design values would best be determined for each application, depending on the vessel's operational profile.

Table 1: Examples of Bulbous bow collision loads from Eqn (17)

Ship Mass Mship [kt]	Ship Speed Vship [m/s]	Ice Mass Mice [kt]	Bulb radius R [m]	Ice Strength Po [MPa]	Ice expon. ex	Ice Force Fn [MN]	Ice pen. [m]	Area [m2]	max accel [m/s2]
100	2	10	1.5	4	-0.1	32	1.1	10.1	0.3
100	4	10	1.5	4	-0.1	62	2.2	21.0	0.6
100	8	10	1.5	4	-0.1	120	4.6	43.6	1.2
100	2	100	1.5	4	-0.1	72	2.6	24.8	0.7
100	4	100	1.5	4	-0.1	139	5.5	51.5	1.4
100	8	100	1.5	4	-0.1	268	11.3	106.9	2.7
100	2	1000	1.5	4	-0.1	96	3.6	34.0	1.0
100	4	1000	1.5	4	-0.1	184	7.5	70.6	1.8
100	8	1000	1.5	4	-0.1	356	15.5	146.4	3.6
100	4	100	1.5	2	-0.1	97	7.9	74.2	1.0
100	4	100	1.5	4	-0.1	139	5.5	51.5	1.4
100	4	100	1.5	8	-0.1	200	3.8	35.8	2.0
100	4	1000	1.5	2	-0.1	128	10.8	101.7	1.3
100	4	1000	1.5	4	-0.1	184	7.5	70.6	1.8
100	4	1000	1.5	8	-0.1	266	5.2	49.0	2.7
100	4	10	1.5	2	-0.1	43	3.2	30.3	0.4
100	4	10	1.5	4	-0.1	62	2.2	21.0	0.6
100	4	10	1.5	8	-0.1	89	1.5	14.6	0.9

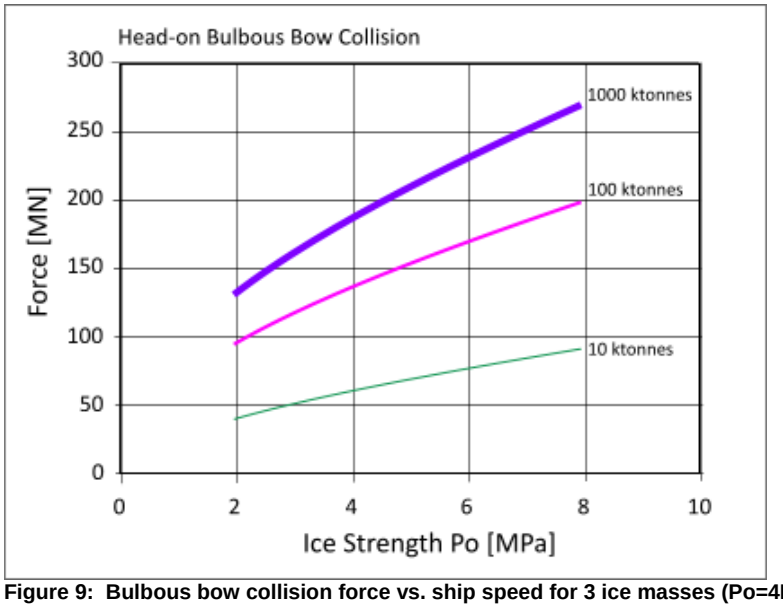

Figure 9: Bulbous bow collision force vs. ship speed for 3 ice masses (Po=4MPa).

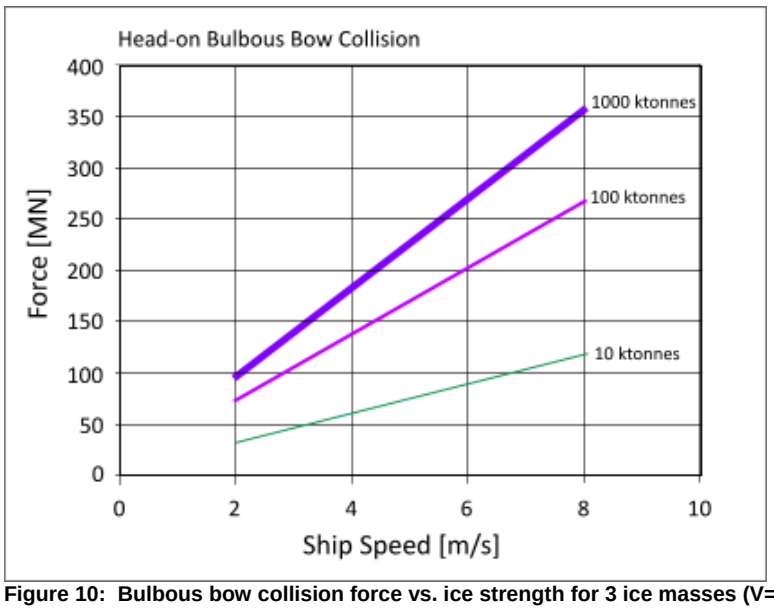

Figure 10: Bulbous bow collision force vs. ice strength for 3 ice masses (V=4m/s).

Aft body Glancing Loads

Another operational scenario involves a collision on the aftbody. In this case the impact velocity will depend on turning rate, and is higher aft of amidships. Vessels with greater turning ability, such as those with azimuthing thrusters, should be given special attention regarding this scenario. In the aft body glancing scenario the side of the ship is assumed to be vertical. The ice edge is assumed to be a simple wedge (see Figure 11), and the ice crushing force is described with a pressure-area model. The intensity of the impact will therefore vary with the normal impact velocity and with the thickness of the ice. Table 2 shows a variety of results. All results assume Po=1.3 MPa, ex =-.1, and ϕ = 150 deg.

The energy balance is expressed in the equation;

$$\frac{1}{2} M_{es} \cdot V_n^2 = \frac{p_o}{2+ex} \left(2h \tan \frac{\phi}{2} \right)^{1+ex} \zeta^{2+ex} \qquad (18)$$

Solving the equation gives the penetration;

$$\varsigma = \left(\frac{2+ex}{2 \cdot p_o \cdot \left(2h \tan\frac{\phi}{2}\right)^{1+ex}} \frac{1}{\frac{1}{M_{es}} + \frac{1}{M_{ice}}} \cdot V_n^2 \right)^{\frac{1}{2+ex}} \qquad (19)$$

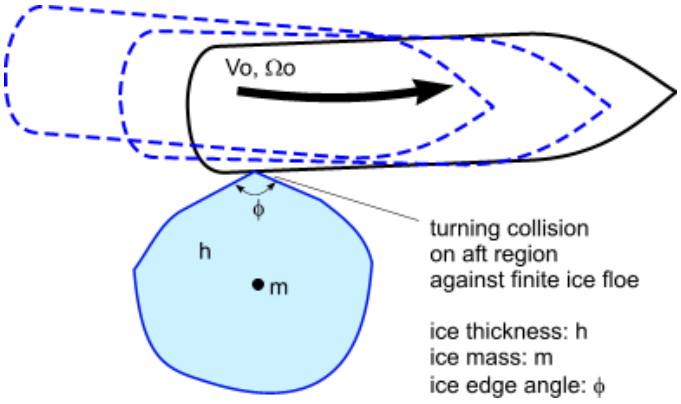

Figure 11. Aft-body glancing collision with an ice floe during a turn.

The force is found by substituting (19) into(10);

$$F_n = p_o \left(2h \tan\frac{\phi}{2}\right)^{1+ex} \cdot \left(\frac{2+ex}{2 \cdot p_o \cdot \left(2h \tan\frac{\phi}{2}\right)^{1+ex}} \frac{1}{\frac{1}{M_{es}} + \frac{1}{M_{ice}}} \cdot V_{ship}^2 \right)^{\frac{1+ex}{2+ex}} \qquad (20)$$

Table 2: Examples of Aft body collision loads from Eqn (20)

Ship Mass Mship [kt]	Ship Fwd Speed Vship [m/s]	Ship Turn Radius [m]	Ship Sway Speed Vsway [m/s]	Dist aft of mid [m]	Ship normal speed Vn [m/s]	Normal Ship Mass Mes [kt]	Ice Thk h [m]	Floe length W [m]	Ice edge angle ϕ [deg]	Ice Mass Mice [kt]	Ice Force Fn [MN]
100	2	1300	0.1	108	0.266	43.0	0.7	100	150	7	1.6
100	4	1300	0.1	108	0.43	43.0	0.7	100	150	7	2.6
100	8	1300	0.1	108	0.76	43.0	0.7	100	150	7	4.5
100	2	1300	0.2	108	0.37	43.0	0.7	100	150	7	2.2
100	4	1300	0.2	108	0.53	43.0	0.7	100	150	7	3.2
100	8	1300	0.2	108	0.86	43.0	0.7	100	150	7	5.0
100	2	1300	0.2	108	0.37	43.0	0.7	100	150	7	2.2
100	4	1300	0.2	108	0.53	43.0	0.7	100	150	7	3.2
100	8	1300	0.2	108	0.86	43.0	0.7	100	150	7	5.0
100	4	1300	0.2	108	0.53	43.0	0.7	100	150	7	3.2
100	4	1300	0.2	108	0.53	43.0	0.7	100	150	7	3.2
100	4	1300	0.2	108	0.53	43.0	0.7	100	150	7	3.2
50	2.9	1030	0	84	0.24	22.1	0.5	100	150	5	1.0
50	1.5	1030	0	84	0.12	22.1	1	100	150	10	1.0
50	0.9	1030	0	84	0.07	22.1	2	100	150	20	1.0
10	3.5	600	0	51	0.30	4.2	0.5	100	150	5	1.0
10	2.2	600	0	51	0.19	4.2	1	100	150	10	1.0
10	1.5	600	0	51	0.13	4.2	2	100	150	20	1.0

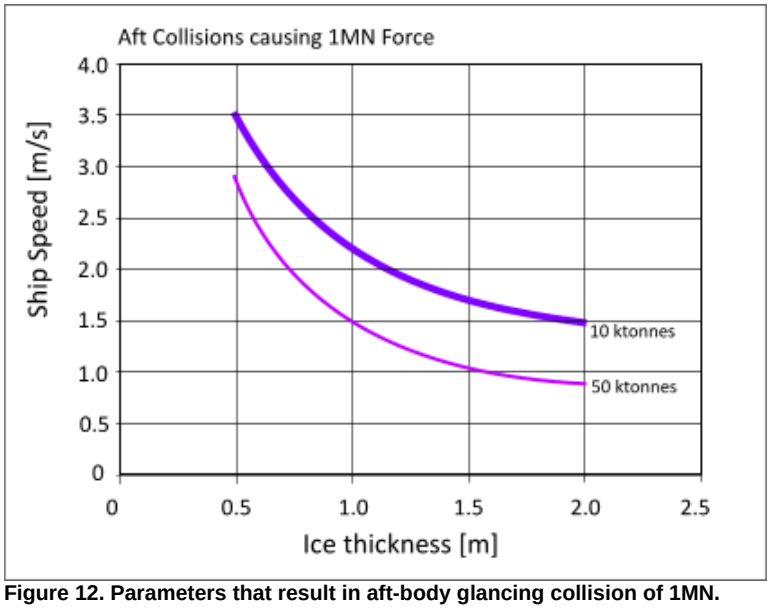

Figure 12. Parameters that result in aft-body glancing collision of 1MN.

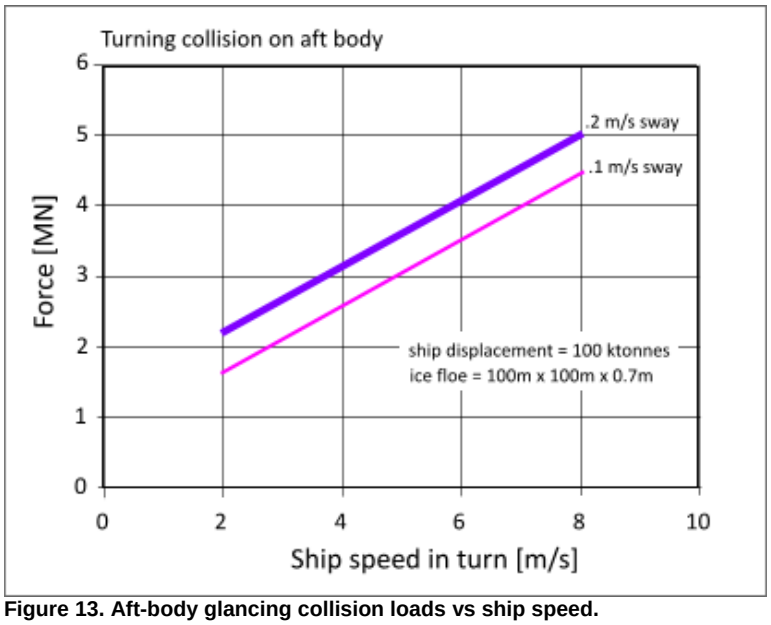

Figure 13. Aft-body glancing collision loads vs ship speed.

Some of the example results from Table 2 are plotted in Figures 12 and 13. Figure 12 shows combinations of parameters that result in a 1MN force. The result indicates that larger ships of the same strength as small ships would need to operate more cautiously. The model could be used to check and improve rule requirements to ensure that displacement effects are properly accounted for in various hull areas. The current Polar Rules tend to use the same displacement effects for all hull areas regardless of the differences in scenarios. Figure 13 shows the influence of both forward speed (assuming a constant turning circle) and side sway on collision loads in impacts with small ice floes.

Influence of Moving Loads on Plastic Structural Response

A large moving load is characterized by an initial collision and subsequent scoring damage. This type of load is a progressive load that causes progressive damage. Progressive damage occurs after the initial ice impact, and can be viewed as plastic structural damage due to the scoring action of ice as it scrapes along the hull. This type of structural interaction can happen at the waterline or below. Waterline damage may result from collision with pack ice, glacial ice of various size (from growler to iceberg), or level ice during ice-channel navigation (assisted or unassisted). Damage below the waterline may occur from collision with glacial ice or if a ship strikes a submerged ice ridge.

Progressive damage is similar to raking damage; however, the tearing and subsequent curling of the hull steel is not treated because ice-strengthened ships are expected to survive such impacts (within their operational capacity) without tearing of the hull plating.

As mentioned previously, common design scenarios call for a static load to be applied to a ship's structure. The effects of any prior damage to the structure are generally not considered. Real-world ice-loads are rarely statically applied, and they commonly involve some degree of scoring damage. In the case of a ship-iceberg collision, the inertia of the ship and the iceberg are comparable, and sustained contact/scoring-damage may occur.

Investigation into the structural reaction of an "IACS polar class" large grillage structure to progressive damage was performed using an explicit dynamics nonlinear numerical model (Quinton 2009). This numerical model was validated against experiments (Daley and Hermanski 2008) involving a full-scale "IACS polar class" large grillage structure. Eight progressive damage load scenarios were investigated (Table 3) using the numerical model. Strategically placed static loads were also simulated in order to provide a basis for comparison between the structure's responses to progressive and static loads.

Table 3. Progressive damage design scenarios investigated.

Category	Scenario
Between Transverses	Between Longitudinals
	Along Longitudinals
	Diagonally Across Longitudinals
Across Transverses	Between Longitudinals
	Along Longitudinals
	Diagonally Across Longitudinals
Perpendicular to Transverses	Between Transverse
	Along Transverse

The results of the load scenarios investigated show a general decrease in the capacity of the "IACS polar class" large grillage structure to carry large progressive loads, versus large static loads. The level of decrease in structural capacity was found to depend on the depth of indentation into the structure, the location of the progressive damage, and the extent of the progressive damage. The structural mechanisms associated with this decrease arise at the transition from a static to a progressive load (i.e. from an impact to a scoring load). Static loads were shown to induce a symmetric structural response throughout the structure adjacent to the load (where permitted by the geometry of the structure). Upon commencement of the large progressive load, this symmetry vanished. The magnitude of the associated bending moments, membrane stresses, and through-thickness shear reactions were all generally smaller on the trailing side of the progressive load than on the leading side. Further, previous plastic damage to large structural members (such as the transverse frames) was shown to have a definite weakening effect on the capacity of the structure adjacent to them.

The numerical simulations were performed using a deformable ship's structure and a rigid indenter. The displacement of the indenter was controlled, and load was transferred to the structure using a surface-to-surface contact algorithm. The method of loading was divided into three actions: initial static loading, progressive loading, and unloading. The static loading consisted of moving the indenter into the hull plating (in a direction normal to the hull plating). This provided a response equivalent to any standard static load scenario. The progressive loading consisted of moving the indenter laterally along the hull plating, thus dragging the initial static indentation along the hull. The unloading consisted of moving the indenter out of the hull plating and releasing the structure.

Figure 14 shows the structure's reaction force (in the direction normal to the hull plating) versus lateral (i.e. dragged) displacement. The imposed progressive loads had hull indentations of 0.2 and 0.5 cm. These loads were imposed on the hull plating between two transverse stiffeners and between two longitudinal stiffeners, and then dragged longitudinally. The start and finish locations of the progressive loads were symmetric about the centre of the structure. The structure is symmetric about its lateral axes. The 0.2 cm load case in Figure 14 exhibits a "bowl-shaped" reaction curve because the overall structural response is elastic (the progressive load is small). The 0.5 cm load case has its initial load higher than its final load. If the structure was loaded statically at both locations, the reactions would be identical due to the symmetry of the structure. The fact that they are not equal in Figure 14 indicates that the progressive nature of the load affected the overall response of the structure. These unequal responses result from prior plastic damage done to the structure as the load progressed to its final position.

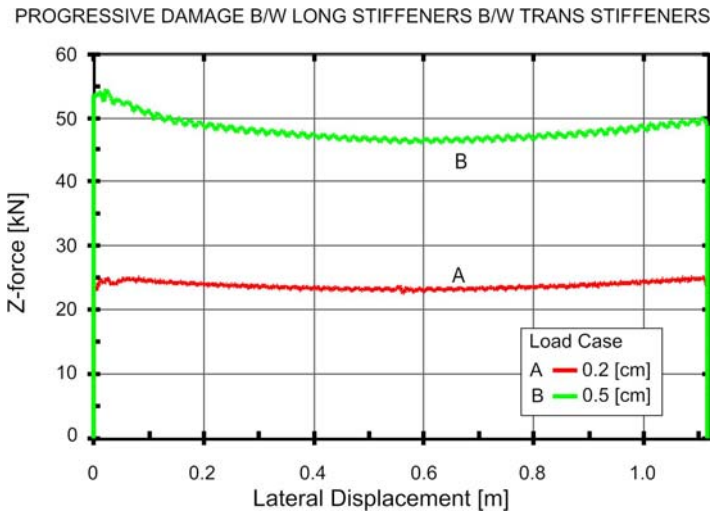

Figure 14. Reaction force versus lateral load displacement for 0.2 and 0.5 cm (indentation) progressive loads.

In addition to the 0.2 and 0.5 cm load cases shown in Figure 14, Figure 15 shows structural reaction curves for 2, 5 and 10 cm load cases. For these large progressive loads, a distinct and immediate drop in structural capacity is observed upon commencement of the progressive loading. The initial plastic damage was much greater for these load cases than for the 0.2 and 0.5 cm load cases. This large amount of initial plastic damage caused an asymmetric structural reaction as the load began to move. Essentially, because the structure on the trailing side of the progressive load was plastically damaged, its ability to exert a reaction force on the indenter via bending and through-thickness shear was compromised; and the reaction force was provided primarily by the undeformed structure on the leading side of the progressive load.

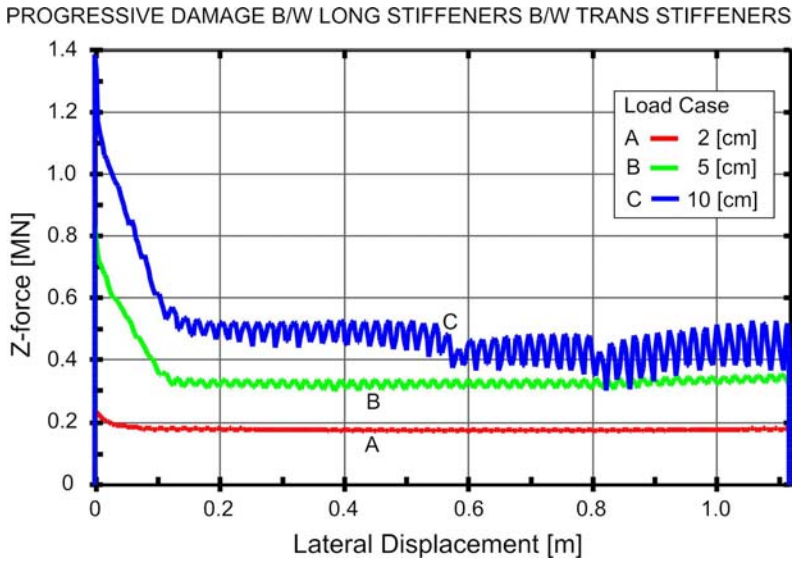

Figure 15. Reaction force versus lateral load displacement for 2, 5, and 10 cm (indentation) progressive loads.

Figure 16 presents the results of a scenario where progressive loads were applied along a longitudinal stiffener that crossed two transverse frames. The results of the numerical model were not valid for the 5 and 10 cm load cases and hence are left out of this figure. The humps in the curves, of course, correspond to the encounters between the indenter and the transverse stiffeners. The 0.2 and 0.5 cm load cases show a relatively elastic overall reaction and exhibit “bowl-shaped” response curves between transverse stiffeners. As above, the large (2 cm) progressive load case shows an initial decrease in capacity upon commencement of the progressive load, and the onset of stiffener buckling as the indenter approaches the transverse stiffeners. In addition to the decrease in bending and through-thickness shear capacity outlined previously, stiffener buckling was observed at a much lower level of indentation for progressive loads than for static loads.

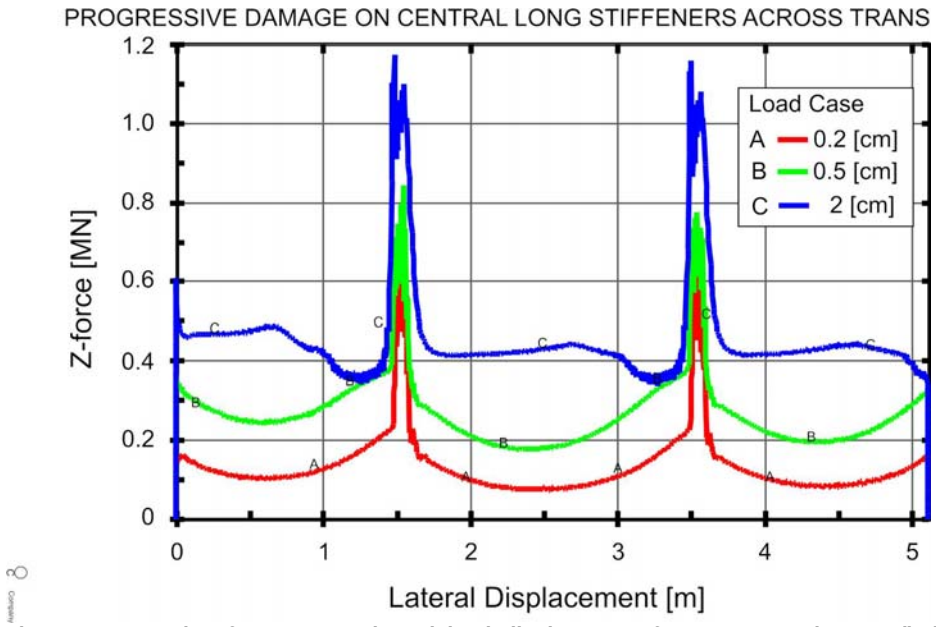

Figure 16. Reaction force versus lateral load displacement for 0.2, 0.5 and 2 cm (indentation) progressive loads that cross transverse stiffeners.

Conclusion

The above illustrate aspects of the direct design and assessment of polar class ships. Ship-ice interactions can be readily simulated using analytical energy methods. This allows the various design and operational parameters to be examined and considered. Both the bulbous bow impact with bergy bits and the aft body impact with ice floes have recently been identified as being of significant importance to the cost and safety of large arctic vessels. The tools described above add to the set that can be applied to these problems.

The final part of the paper takes the analysis to the next step, that of determining structural response. The results, though preliminary, do illustrate the need to consider the effects of moving loads on the plastic response. It appears that moving loads may cause significantly more structural damage than purely normal loads. This effect is one that requires further consideration as plastic design is increasingly employed.

References

Daley, C., Hermanski, G., (2008) “Ship Frame Research Program - An Experimental Study of Ship Frames and Grillages Subjected to Patch Loads, Volumes 1 and 2”, Ship Structure Committee, SSC Project SR 1442 - Final Report; OERC Report 2008-001; NRC-IOT Report TR-2008-11.

Daley, C., Kendrick, A., (2008) "Direct Design of Large Ice Class Ships with Emphasis on the Midbody Ice Belt" Proceedings of the 27th International Conference on Offshore Mechanics and Arctic Engineering, July 15-20, 2008, Estoril, Portugal, OMAE2008-57846

Daley, C., Kendrick, A., Yu, H., Noh, B-J., (2007) “Structural Design of High Ice Class LNG Tankers”, RINA Conference Design & Construction Of Vessels Operating In Low Temperature Environments 30 - 31 May 2007, RINA HQ, London, UK.

International Association of Classification Societies (2007), “Requirements Concerning Polar Class”, www.iacs.org.uk

Daley, C.G., (2000) “Background Notes to Design Ice Loads - IACS Unified Requirements for Polar Ships” Prepared for IACS Ad-hoc Group on Polar Class Ships and Transport Canada, February 2000

Daley, C.G., (1999) “Energy Based Ice Collision Forces” – POAC ’99, Helsinki Finland, August 1999.

Popov, Yu., Faddeyev, O., Kheisin, D., and Yalovlev, A., (1967) "Strength of Ships Sailing in Ice", Sudostroenie Publishing House, Leningrad, 223 p., Technical Translation , U.S. Army Foreign Science and technology Center, FSTC-HT-23-96-68.

Quinton, B. (2009). “Progressive Damage to a Ship's Structure due to Ice Loading”, M. Eng., Memorial University of Newfoundland